scientific reports

Check for updates

OPEN

Spatial and seasonal fluctuations in fresh submarine groundwater discharge revealed by marine continuous resistivity profiling

Jose Tur-Piedra[1,2]✉, Juanjo Ledo[3], Marc Diego-Feliu[1,2], Pilar Queralt[4], Alex Marcuello[4], Valentí Rodellas[5] & Albert Folch[1,2]

Submarine Groundwater Discharge (SGD) is a major pathway for the discharge of fresh and saline groundwater and associated dissolved compounds into marine environments. However, assessing SGD processes in coastal aquifers is challenging due to inaccessibility, dynamic conditions, complex subsurface geology, and the need for long-term monitoring to capture temporal and spatial variations in SGD rates accurately. This study employs marine continuous resistivity profiling (MCRP) as a main method to assess the presence of freshwater or brackish SGD offshore and to examine its potential seasonal variations. The method has been applied in the coastal alluvial aquifer of Maresme (Spain) and validated with other methods to trace SGD, including salinity profiles, Ra isotopes, and piezometric levels. Several MCRP transects of 700 m long, perpendicular to the coastline, were performed in a coastal marine area to obtain electrical resistivity data of the seabed covering an area of 3 km^2. The data was acquired in two field campaigns with contrasting hydrological conditions (dry and wet seasons). The MCRP results allow the identification of areas of fresh SGD in marine sediments, with a clear seasonal variability that indicates a higher discharge of fresh groundwater in the wet season.

Keywords Marine geophysics, SGD, Seasonality, Mediterranean sea, Electrical resistivity tomography, Coastal groundwater

Submarine Groundwater Discharge (SGD) is an important process regulating the transfer of nutrients, metals, pollutants, and other dissolved compounds from land to ocean[1–3]. The significance of the process stems from its environmental and social implications; it is vital for sustaining entire ecosystems and providing different ecosystem services for society[4–6]. SGD is a complex hydrological process that involves the discharge of meteoric fresh SGD (FSGD) and recirculated seawater (RSGD)[7]. While global estimates of FSGD indicate that the process is volumetrically insignificant on a global scale relative to RSGD (< 1%), itis locally an important process delivering new nutrients to the coastal ocean[3,8], especially in areas where there are no contributions from surface watercourses.

FSGD varies spatially and temporally due to inland and ocean physical forces and aquifer characteristics[9]. Terrestrial factors consist of hydraulic gradients, influenced by seasonal changes and human activities, and the geological characteristics of the aquifer. Oceanic factors involve density-driven convection, tidal changes, and wave activity. Together, these factors regulate the flow of groundwater to the sea, affecting SGD rates and distribution[7,10,11]. It is, therefore, fundamental to develop approaches to capture the spatial and temporal variations of FSGD.

Local SGD investigations are often focused on the quantification of total SGD flows without distinguishing the contribution of fresh groundwater and identifying the preferential discharge areas[12,13]. Remote sensing techniques, such as satellite imagery and thermal infrared data, can effectively identify potential SGD sites by detecting surface anomalies like temperature variations[14–16]. Spatial analysis of chemical tracers of SGD (e.g. salinity, radon) can also be used to identify the location of fresh SGD inputs from measurements in surface waters[17,18]. In contrast, geophysical techniques are instrumental in identifying and delimiting freshwater

[1]Department of Civil and Environmental Engineering (DECA), Universitat Politècnica de Catalunya (UPC), Barcelona 08034, Spain. [2]Associated Unit: Hydrogeology Group (UPC-CSIC), Barcelona, Spain. [3]Department of Earth Physics and Astrophysics, Faculty of Physics, Universidad Complutense de Madrid, Madrid, Spain. [4]Department of Earth and Ocean Dynamics, Faculty of Earth Sciences, Universitat de Barcelona, Barcelona, Spain. [5]Department of Physics, Universitat Autònoma de Barcelona, Bellaterra, Spain. ✉email: jose.tur@upc.edu

and saltwater in coastal subsurface. Electrical and electromagnetic methods are particularly effective for characterizing FSGD, as they can detect changes in electrical resistivity associated with variations in salinity[19].

The use of electrical geophysical techniques has been commonly employed in coastal areas to characterize aquifers and map freshwater, seawater, or their mixture, as well as changes in porosity[20–22]. In nearshore environments, FSGD or saltwater–freshwater dynamics have been studied using stationary marine electrical resistivity in which electrodes are submerged and come into contact with sediment at a fixed position on the shoreline[23,24]. In offshore areas, other studies have been conducted using marine continuous resistivity profiling (MCRP), in which floating electrodes are towed with a boat[19,25–27]. The MCRP has proven to be effective in studying salinity distribution in marine sediments and potential discharge areas in different marine environments, such as bays like Florida Bay in the United States[28] or Jobos Bay in Puerto Rico[25], as well as in marine reef areas such as Santiago Island in the Philippines[11,26] or on the coast of Belgium[19].

The MCRP has been applied in conjunction with other geophysical techniques such as stationary marine electrical resistivity[28], terrestrial electrical resistivity tomography and electromagnetic frequency domain[19] to characterize FSGD, allowing for the integration of information obtained from different methods. MCRP has also been applied in order to characterize SGD using a variety of different and complementary methodologies, such as SGD tracers like Ra isotopes and Rn, dissolved O_2, temperature, and salinity[20,29]. These studies have employed MCRP to capture subsurface electrical resistivity at a single moment, enabling the acquisition of snapshot observations of FSGD. However, this method has not been tested to assess temporal variations of FSGD.

This study aims to evaluate seasonal and spatial variations of FSGD through MCRP in a shallow coastal area along the western Mediterranean Sea. Fieldwork was conducted in the Maresme region, northwest of Barcelona (Spain), during the dry and wet seasons in 2020. MCRP results have been complemented and validated using other methods, such as piezometric level evolution, salinity profiles, and Ra isotopes.

Study area

The study area is located in the Maresme region, 40 km northeast of Barcelona (Spain, western Mediterranean Sea) (Fig. 1). This region extends along the coastal slope of the Catalan Coastal Range, the mountain chain that runs parallel to the coast in a SW-NE orientation and reaches heights of up to 600 m. The Catalan Coastal Range was formed during the Paleogene due to regional compressive tectonic activity and a subsequent distensive phase during the Neogene. The geology of the area consists of two main units: a Hercynian granitic basement that outcrops in the upper part of the range and Quaternary alluvial deposits forming the coastal plain, composed of weathered materials from the same range (Colombo & Rivero, 2017). These alluvial deposits consist of gravel, sand, and sandy silt intercalations associated with intermittent surface water courses extending towards the coast[30]. The seabed of the region is formed by deposits of unconsolidated coarse sand derived from weathered granite, transported by intermittent watercourses. These sand deposits alternate with the appearance of beachrocks, consisting of ancient beach sands cemented by precipitation of calcium carbonate. These beachrocks are submerged due to successive phases of sea level rise[31]. This presence of consolidated materials, parallel to the current coastline, causes changes in the relief of the seabed.

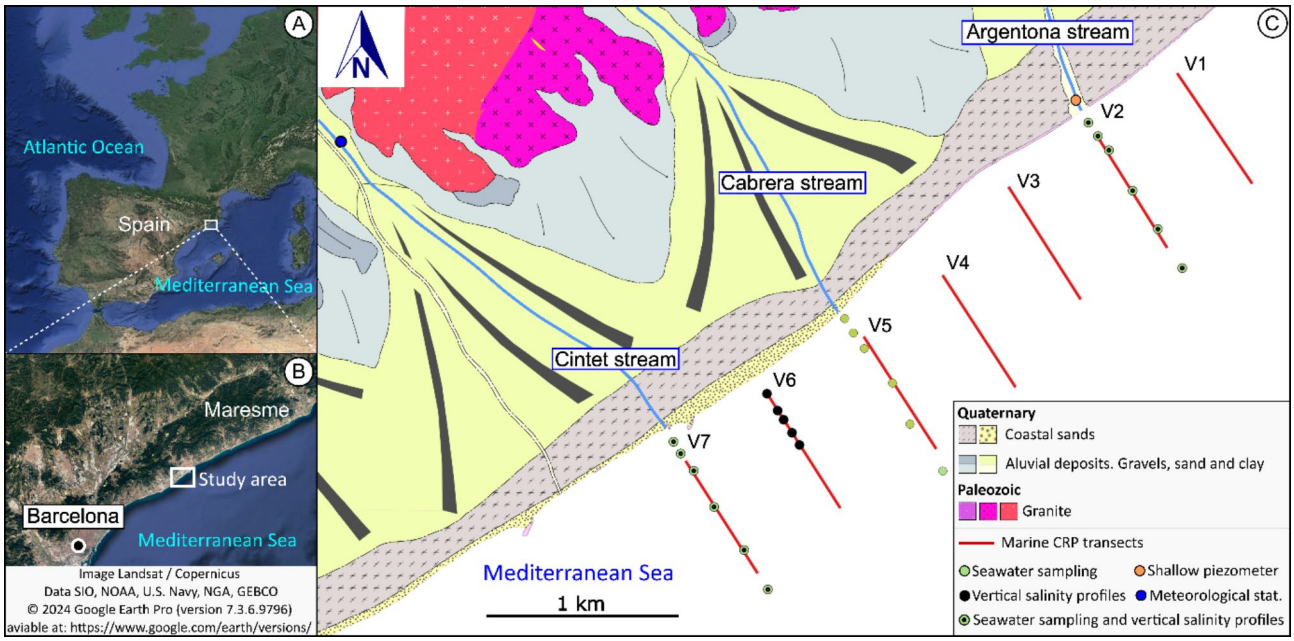

Fig. 1. The study area is located in the NW Mediterranean basin, 40 km northeast of Barcelona. Location map (**A**), regional map (**B**) and experimental setup description (**C**) of the study site with the geological context, location of MCRP transects (red lines), the position of salinity profiles performed (green dots) and the inland shallow piezometer (orange dot). Location and regional map generated with Google Earth Pro software[32].

Hydrogeologically, the presence of silty layers implies a low hydraulic conductivity, while the sand and gravel levels have a very high hydraulic conductivity[33]. These alluvial levels have continuity from land to sea and can form structures such as paleochannels and small lobes or deltas. This connection, which can be very complex in all three dimensions, allows a preferential groundwater circulation. Local studies show that the aquifer has the dynamics of a multi-aquifer system, in which freshwater is expected to be discharged into the sea at various depths and distances from the coast[22,34,35]. Accordingly, Ra isotope activity has been found to be high at the first 400 m off the coast, indicating that SGD occurs not only on the coastline but also offshore[36].

This area has a Mediterranean climate, with average temperatures of 12 ºC in winter and 21 ºC in summer. In the coastal zone, the irregular rainfall, which can be periodically intense, ranges from 350 $mm{\cdot}a^{-1}$ in the driest years to 930 $mm{\cdot}a^{-1}$ in the wettest (in the 2015–2020 period). These irregular precipitations imply variations in aquifer recharge, being more significant in spring and autumn and relatively low during summer. In this research, the first campaign took place in the dry season (June 2020) and the second one was carried out during the rainy season (October 2020), after a period of rain in the previous weeks. According to the Meteorological Catalan Service[37], in the municipality of Cabrils (located 4 km away) the accumulated rainfall in this region in the five days previous to the campaign amounted to 58.3 mm, approximately 8%of the annual precipitation in 2020.

Methods

In this study, two field campaigns in June and October 2020 were carried out to identify FSGD variations, mainly through changes in resistivity in the marine sediment. MRCP data was complemented and validated with the measurement of piezometric levels, shallow salinity measurements, and vertical salinity profiles, as well as the analysis of radium isotopes during the wet season. The study area spans roughly 3 km along the coastline and extends 1 km offshore.

Data for MCRP was acquired along seven transects perpendicular to the coast along NW-SE direction (V1, V2, V3, V4, V5, V6, V7) and repeated over the two campaigns (Fig. 1). Each transect is 700 m long and the shore-parallel separation between transects is approximately 500 m (Fig. 1). They start at 150–200 m from the coastline, where the water column depth is about 3 m, and the offshore section is about 850–900 m from the coastline, with water column depths of about 10 m. The total linear distance of the set of transects is around 5 km.

Inland piezometric level

A CTD-Diver DI272 (Schlumberger™) was placed in a well located at the mouth of the Argentona stream (see Folch et al. 2020 to obtain information on the experimental site) to obtain continuous information on the piezometric levels, electrical conductivity and temperature for the whole of 2020, including both field surveys.

Seawater salinity measurements

A CTD-Diver DI271 (Schlumberger™), attached to the multi-electrode marine cable, monitored conductivity and temperature changes in seawater during navigation. Data was recorded every 30 s at a depth of 20 cm below sea level (Fig. 2). The sea surface conductivity averaged 54.5 $mS{\cdot}cm^{-1}$ in both campaigns, indicating an electrical resistivity of 0.18 ohm·m. This value is utilized for the water layer in electrical resistivity models.

During the October 2020 campaign, a CTD-Diver DI271 (Schlumberger™) was employed along transects V2, V6, and V7 to measure vertical salinity profiles (SP) of seawater at different distances from the coast, aiming to detect vertical salinity fluctuations attributed to FSGD. Salinity profiles were conducted at specific distances offshore: at 75, 150, 250, 500, 750, and 1000 m for transects V2 and V7, and at 150, 250, 300, 400, and 500 m for transect V6 (see Fig. 1).

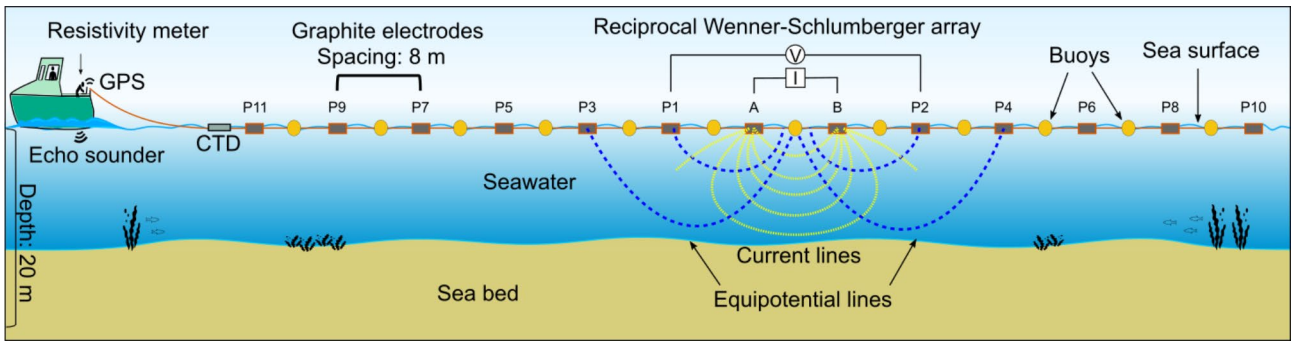

Fig. 2. The schematic diagram shows the acquisition of marine continuous resistivity profiling data using a reciprocal Wenner-Schlumberger configuration. Electrodes A–B function as the current electrodes, while electrodes P1–P11 act as potential electrodes. The resistivity system performs ten simultaneous measurements of apparent resistivity up to 20 m deep.

Seawater Ra isotopes activities

In October 2022 (wet season), seawater samples for Ra isotopes (^{223}Ra, ^{224}Ra, ^{226}Ra, and ^{228}Ra) were collected at various stations along two perpendicular transects to the coastline, corresponding to the ephemeral streams of Argentona and Cabrera (designated as Transects V2 and V5, respectively; see Fig. 1). Each transect comprised 7 offshore stations spaced evenly within the first 1000 m. At each station, surface seawater samples were obtained by deploying a submersible pump at a depth of 0.5 m below sea level.

Following collection, the water samples underwent filtration through MnO_2-impregnated acrylic fibers at a flow rate of less than 1 L·min^{-1} to facilitate the quantitative adsorption of Ra isotopes onto the fibers[38]. Subsequently, the fibers were washed with free radium deionized water at the home laboratory and dried to achieve a 1 to 1 fiber–water ratio[39]. Each fiber sample was measured twice using the radium delayed coincidence counter (RaDeCC; Moore & Arnold, 1996). The short-lived Ra isotopes (^{223}Ra, $T_{1/2} = 11.4$ d; ^{224}Ra, $T_{1/2} = 3.66$ d) were quantified based on the initial measurement with the RaDeCC system. However, the activities of ^{223}Ra are not reported in this study due to high ^{224}Ra activities, which interfered with proper quantification, as observed through the cross-talk effect[40].

The second measurement, conducted one month after sampling, aimed to quantify the unsupported activity of ^{224}Ra (excess ^{224}Ra; $^{224}Ra_{ex}$), factoring in the activity of its parent, ^{228}Th, in the fiber. Quantification of ^{224}Ra followed guidelines and limits proposed by Diego-Feliu et al. (2020) to mitigate inherent interferences in the detection system, with uncertainties estimated according to Garcia-Solsona et al. (2008). Subsequently, the MnO_2 fibers were incinerated, ground, and transferred to gamma-counting vials. Following a radioactive equilibration period of 21 days, the activities of the long-lived Ra isotopes (^{226}Ra, $T_{1/2} = 1600$ years; ^{228}Ra, $T_{1/2} = 5.75$ years) were measured using a HPGe gamma spectrometer. Specifically, the photopeaks of ^{214}Pb (352 keV) and ^{228}Ac (911 keV) were utilized to quantify the activities of ^{226}Ra and ^{228}Ra, respectively.

Marine continuous resistivity profiling (MCRP)

MCRP equipment consists of a 10-channel IRIS-SYSCAL PRO resistivity meter (IRIS Instruments, Orleans, France) connected to a 12 V battery and 112 m floating multielectrode marine cable with graphite electrodes, spaced between them 8 m (Fig. 2). The acquisition data configuration used is reciprocal Wenner-Schlumberger. During navigation, the cable is towed with a speed of around 6 km·h^{-1} with the current transmission occurring at intervals of approximately 8 m, obtaining 10 measurements per injection, with an estimated investigation depth of about 20 m. For the computerized acquisition of electrical resistivity data, the computer has specific IRIS Instruments software (Sysmar) from which data logging is controlled. In addition, a GPS (Garmin ECHOMAP™ Plus 42 hp with transducer) was used to georeference the data and a bathymetric probe to obtain bathymetry data during the boat trip.

Slight variations in the navigation course occurred, relative to the design initially proposed, due to multiple causes: maritime traffic, the presence of buoys delimiting bathing areas, the safety margin of the vessel concerning bathymetry, the limited manoeuvrability of the boat, or the effect of the waves and currents. However, the performed transects remained highly consistent with the originally proposed design, resulting in a satisfactory outcome. A diagram of the route taken can be consulted in the supplementary material (Figure SI1). Raw data of apparent resistivity and bathymetry and its positioning are reviewed and edited to ensure data quality, removing some anomalous data (e.g., local negative values or outliers). On average, the skipped data represents less than 2% of the total data acquired.

For the 2D inversion of the data, we have used the smoothed inversion of the AGI EarthImager2D software (Advanced Geosciences Inc.). The initial model for inversions takes the seabed sediments as homogeneous earth with resistivity equal to the average apparent resistivity, and a seawater resistivity of 0.18 ohm·m (average obtained by the CTD). Figure 3 shows the data, the model's responses, and the model for an individual transect (e.g. V2 results of the campaign performed in October 2020). In our results, the Root Mean Square (RMS) error range oscillates between 2 and 6%, and the normalized L2-norm is <1, which is considered a good fit[41]. The seawater layer thickness considers the bathymetry represented with a white line (Fig. 3c).

Resistivity model interpretation

Electrical resistivity methods prove valuable in discerning the presence of freshwater, brackish, or saline water in coastal aquifers. This assessment relies on Archie's law[42]:

$$\rho_b = a\rho_w F, \tag{1}$$

which relates the total resistivity of sediment saturated with water, i.e. bulk resistivity, (ρ_b in ohm·m), tortuosity (a, dimensionless, approximately 1), porewater resistivity (ρ_w in ohm·m), and the formation factor (F, dimensionless).

The formation factor can be defined as $F = \varphi^{-m}$ where φ represents porosity in percentage, and m stands for the cementation exponent (dimensionless). Local studies suggest porosity values ranging from 0.25 to 0.3 and m values between 1.3 and 1.8[22]. Consequently, F may range between 5 and 13. Given the average electrical conductivity of seawater at the study site (54.5 mS·cm^{-1}, which is equivalent to $\rho_w = 0.18$ ohm·m), and considering the range of formation factors, the bulk resistivity of sediments saturated with seawater can vary from 0.90 to 2.3 ohm·m. In previous studies on electrical resistivity of marine sediments[19,27,43] a similar range of values was presented, where values lower than 2 ohm·m indicated saturated sediment with seawater. On the other hand, resistivity values ranging from 2 to 5 ohm·m indicated marine sediment saturated by brackish water.

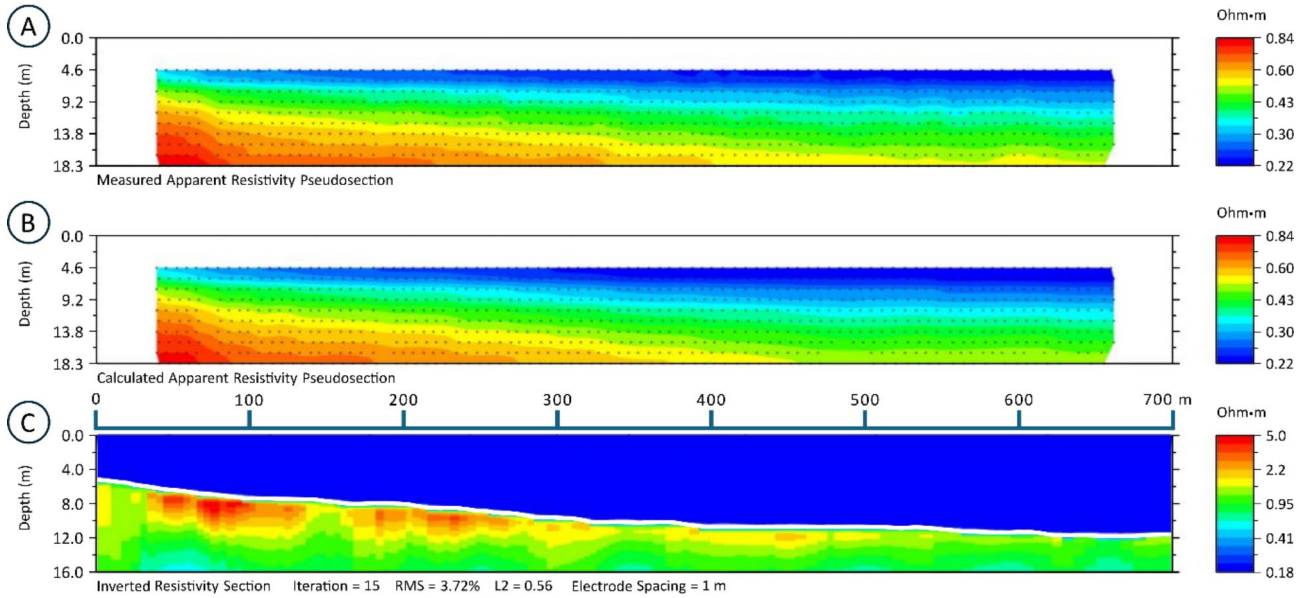

Fig. 3. Example to obtain the electrical resistivity model of a transect with the Earthimager software. (**A**) Raw data in apparent resistivity pseudosection, (**B**) model response in calculated apparent resistivity pseudosection, and (**C**) Electrical Resistivity model.

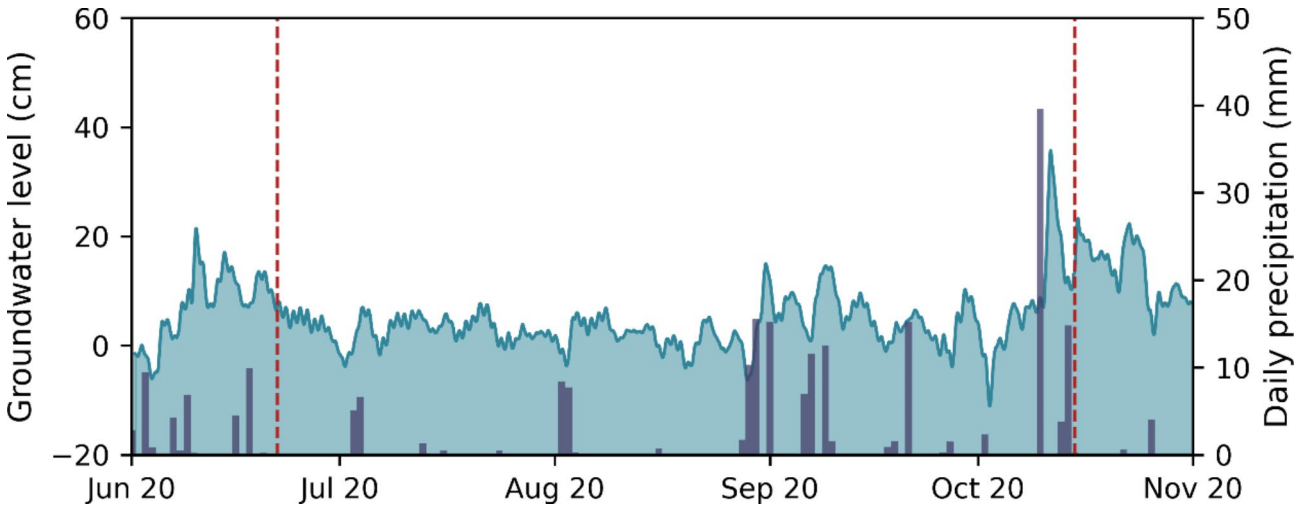

Fig. 4. Temporal evolution of groundwater level from 1st June 2020 to 1st November 2020 at the experimental site of the Argentona ephemeral stream. The red dashed line represents the seasonal campaigns (June and October 2020). Vertical blue lines are daily precipitation from the Cabrils meteorological station. Modified from Diego-Feliu et al. 2022.

Results

Piezometric level

The data obtained from the CTD located in the piezometer at the mouth of the Argentona stream indicates aquifer recharge during the rainy season (Fig. 4). The groundwater level is expressed in terms of relative variation relative to the base flow conditions of March 2020[36]. Although the piezometric level in June is also around 10 cm higher than the base flow of March 2020, the increase in precipitation during wet seasons (especially in October 2020) results in an increase in the piezometric level of up to 23 cm. Notice that the sampling campaign conducted in June is representative of dry season due to the lack of significant precipitation, whereas the sampling in October was conducted after important precipitation events.

Seawater salinity profiles

The results obtained by the CTD salinity profiles along the marine transects fall within a range of values between 38.0 and 38.6 PSU. In all transects, the data shows a trend in which the salinity is slightly lower near the coast

than offshore (Fig. 5). These lower values may be related to the rain of the previous days, but no surface runoff has been observed in the ephemeral streams during the campaign. Furthermore, in some profiles it was also observed that the values close to the seafloor show a decrease in salinity (decrease of 0.2–0.3 PSU), such as in transect V7 (150 m, 250 m and 500 m) and in transect V6 (250 m and 400 m).

Seawater Ra isotopes

Seawater activities of ^{224}Ra and ^{228}Ra in samples collected at stations along the offshore transects (V2 and V5) during the field campaign of October 2020 are depicted in Fig. 6, together with data from two previous campaigns (October 2019 and March 2020) conducted as part of a parallel study aimed at estimating the magnitude of SGD in the area[36]. The activities of Ra isotopes in October 2020 range from 1.5 ± 0.2 to 14.4 ± 1.9 Bq·m^{-3} for ^{224}Ra and 1.2 ± 0.5 to 3.3 ± 0.2 Bq·m^{-3} for ^{228}Ra. Notably, these activities generally decrease with increasing distance offshore along both transects (see Fig. 3). However, the decrease is more pronounced in samples collected at 500 m offshore, which exhibit similar activities to those found in open ocean waters (approximately 1000 m offshore), less than 4 Bq·m^{-3} in ^{224}Ra and near 1 Bq·m^{-3} in ^{228}Ra. It is also noteworthy that the observation of activities during the sampling campaign of October 2020 yield intermediate values up to 500 m from the coast compared to those observed in October 2019, a sampling preceded by an extreme precipitation event, and those in March 2020, which followed a relatively long dry period (an accumulated precipitation of 18 mm in the prior 40 days).

Marine CRP

The results from the 2D inversion models acquired during the dry season show relatively low electrical resistivity values in all models (Fig. 7). These values, in a range between 0.5 and 2 ohm·m, are characteristic of unconsolidated marine sediments saturated by seawater, similar to those found by other authors[25,28]. Despite this, slightly higher resistivity values near the coast suggest that a small proportion of fresh groundwater may be present, even during periods of limited recharge. In the models located south of the study area, a sudden change in bathymetry stands out, with resistivity values between 4 and 5 ohm·m. These changes are likely associated to lithology heterogeneities, such as the presence of previously identified beach rocks near this area[44] which may have resistivity values in this range, as described by Psomiadis et al., 2009.

The October 2020 campaign's models reveal a larger expanse of higher resistivity values in offshore areas. The most prominent area with high resistivity values is in the northern sector of our study area (V1, V2, and V3), where shifts in resistivity have been observed up to 800 m offshore (see Fig. 8). The highest resistivity values are noticeable in the southern models (V5 and V7), with a discernible rise in resistivity values at distances of 400 and 600 m, respectively. When comparing the wet season models with those of the dry season, a significant increase

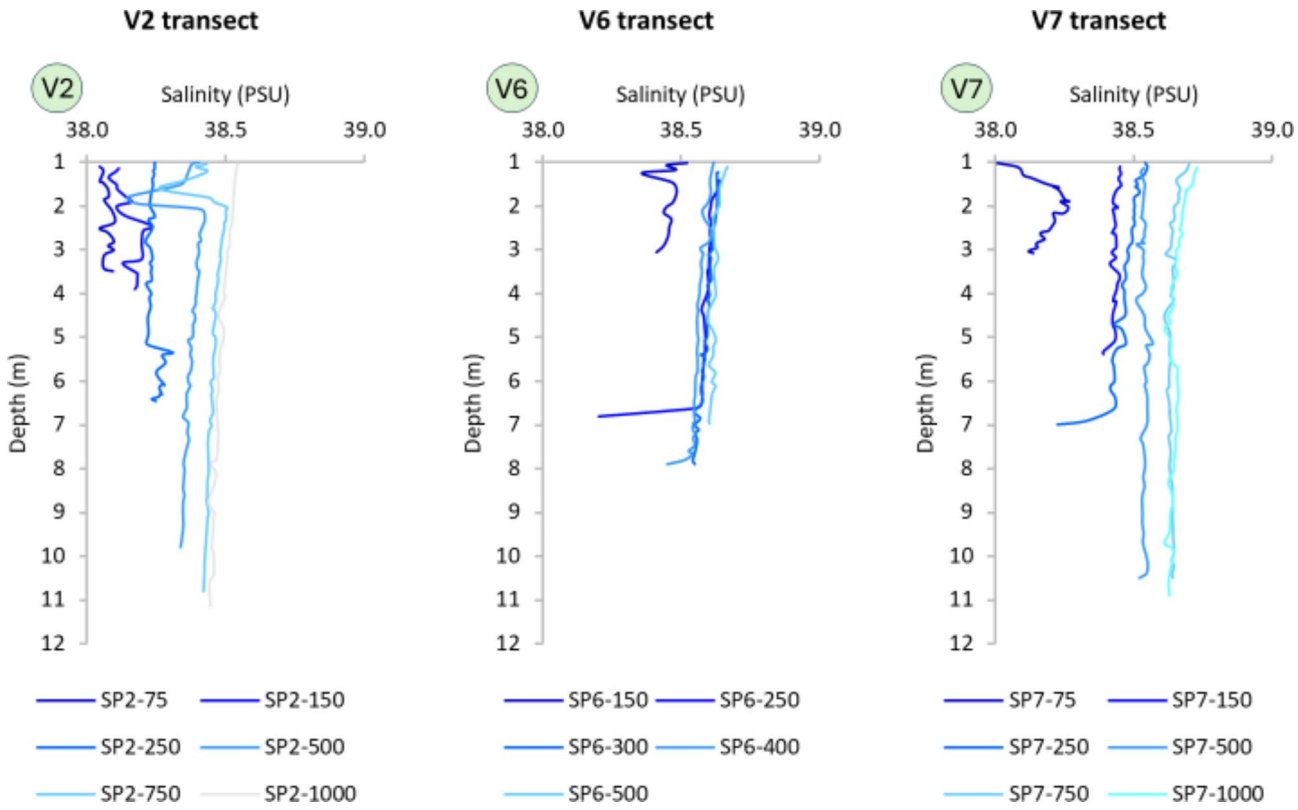

Fig. 5. Salinity profiles performed in V2, V6, and V7 transects at different distances from the coastline (Fig. 1) in October 2020.

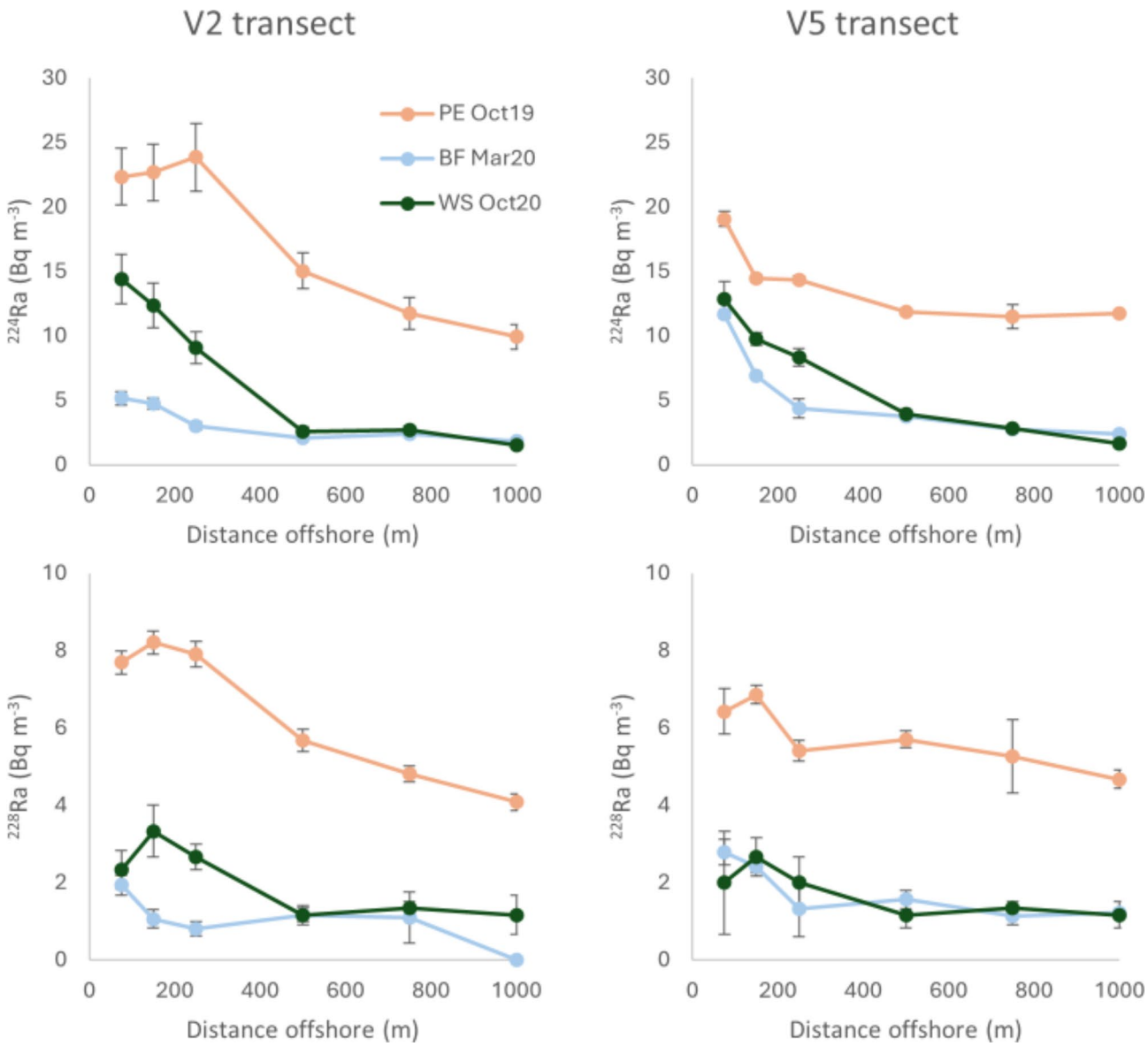

Fig. 6. Radium isotope activities 224Ra and 228Ra in coastal seawater samples collected during the samplings performed during the wet season in October 2020 (WS Oct20) compared with an extreme precipitation event (PE oct19) and March 2020 base flow (BF Mar20) by Diego-Feliu et al. (2022), for two transects perpendicular to the coastline corresponding to the ephemeral streams of Argentona (V2) and Cabrera de Mar (V5).

in resistivity between 2 and 5 ohm·m can be observed in the wet season (represented in red in the models). These resistivity changes occur predominantly between 5 and 15 m depth. The magnitude of this increase varies depending on the location within the study area, since in transects V4 and V6, the resistivity range generally remains below 2 ohm·m.

Discussion

Spatial resistivity changes associated with SGD

The electrical resistivity values within the marine sediments near the coastline present a higher resistivity than the offshore results. This observation suggests a progressive salinity gradient in the subsurface, where the proximal coastal zones have more fresh water. Furthermore, these models reveal the highest resistivity values, predominantly between 5 and 15 m in depth. This distribution implies the possible existence of preferential flowpaths for FSGD which would be in line with the intrinsic geological and hydrogeological heterogeneity of the coastal aquifer system.

When comparing different transects, comparatively higher resistivity values are observed in the northern sector of the study area (V1, V2, and V3). This spatial variation of electrical resistivity values is consistent with the distribution of ephemeral watercourses, as the Argentona stream is located in the north of the study area and its alluvial system has the greatest recharge capacity in the area (Fig. 1). The smaller streams in the south, Cabrera

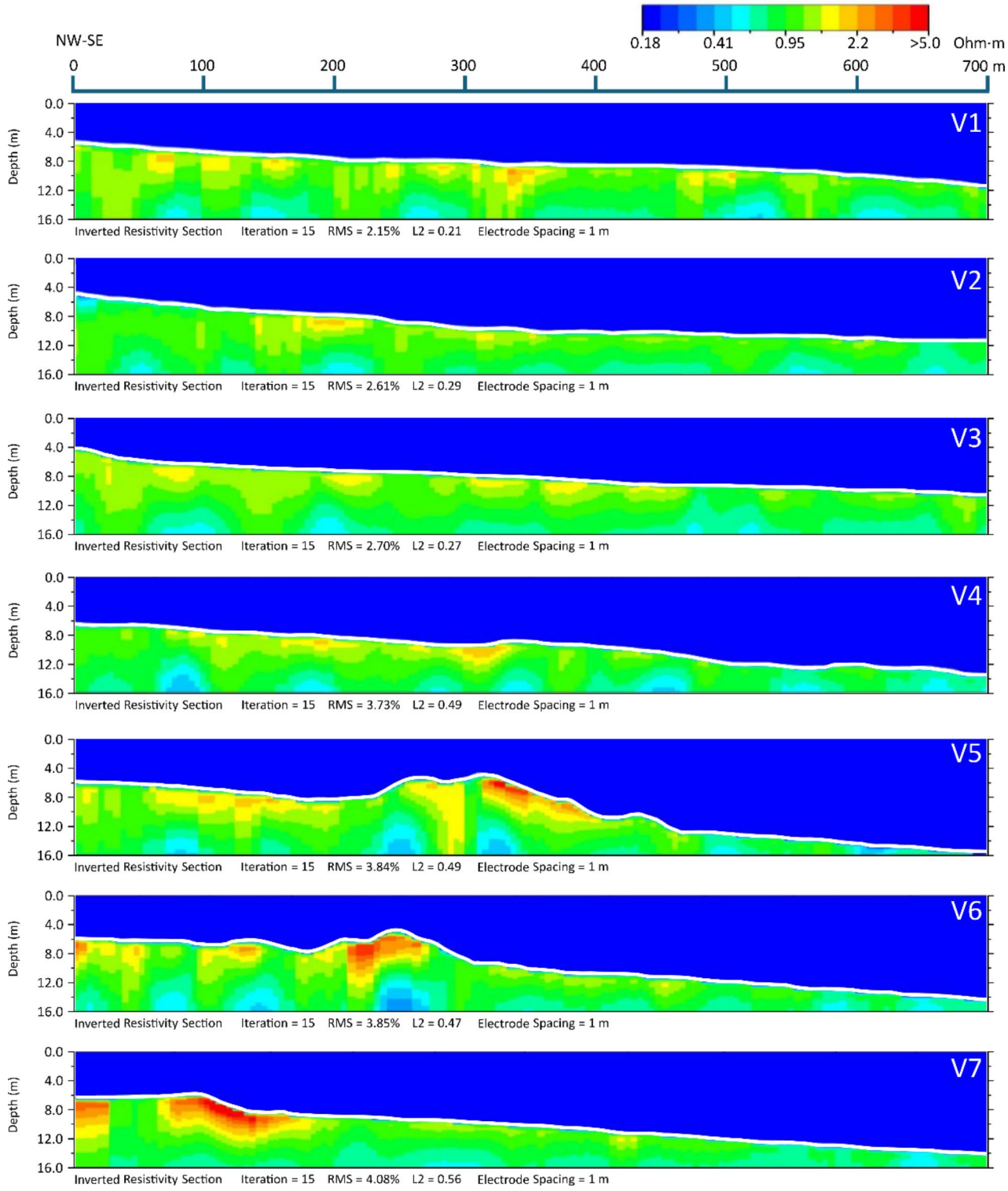

Fig. 7. Electrical resistivity models from the June 2020 campaign. All the models presented have a length of 700 m.

stream (V5) and Cintet stream (V7), also appear to contribute to greater local recharge. Locally, these alluvial deposits have high permeability, allowing rapid movement and dispersion of groundwater, as reflected in[33,35]. This geological context promotes diffuse groundwater discharge, unlike less permeable formations or karst zones that favour focused SGD[45].

The vertical salinity profiles carried out in transects V2, V6, and V7 show salinity changes consistent with offshore FSGD, particularly in V2 and V7 transects. These profiles show a progressive increase in salinity

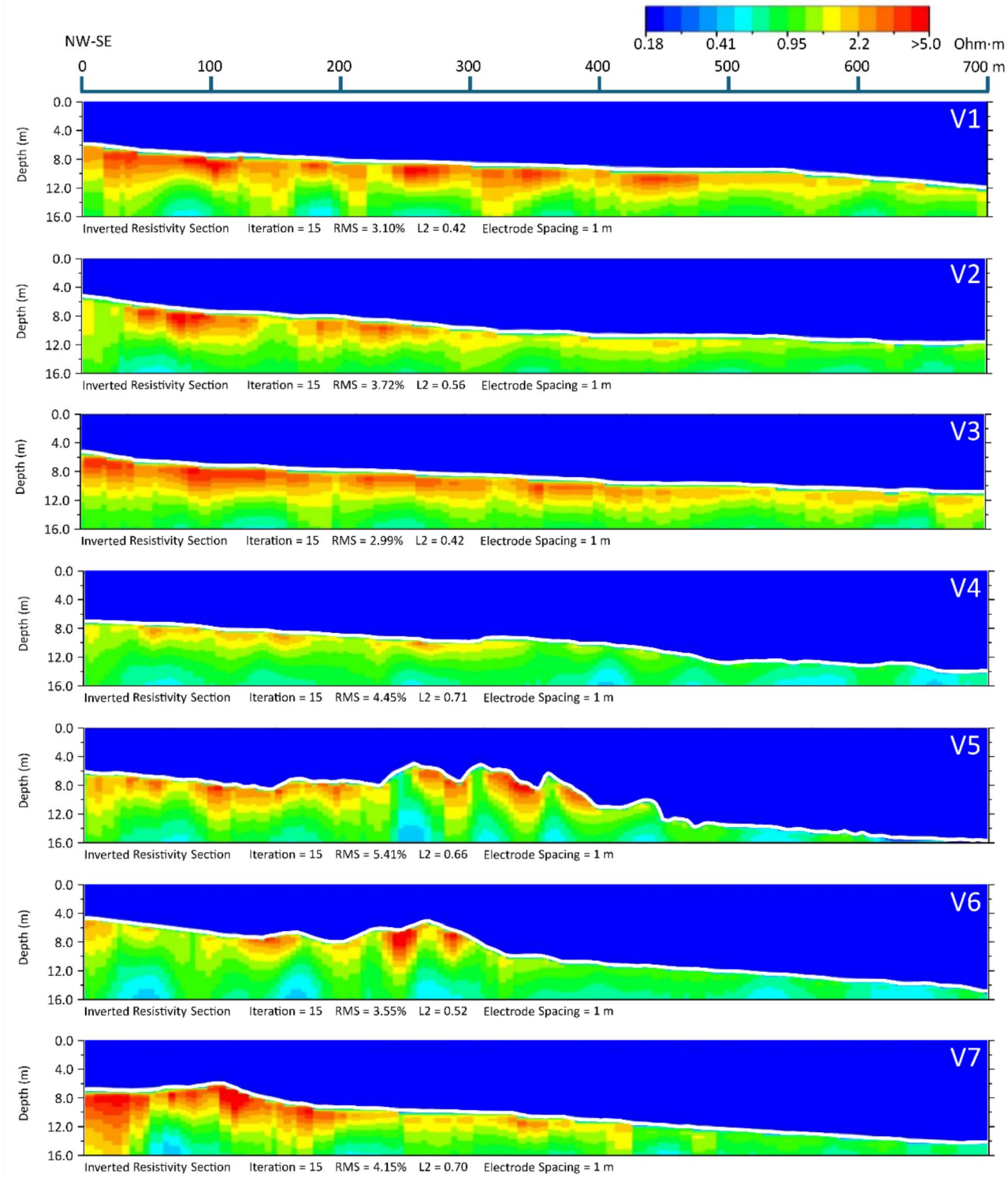

Fig. 8. Electrical resistivity models from the October 2020 campaign. All the models presented have a length of 700 m.

offshore, where the lowest values are found near the coast, consistent with FSGD occurring mainly at nearshore areas. The effect of the rains in the previous days may also justify this reduction in salinity, but there was no evidence of surface runoff in the ephemeral streams during the campaign. Furthermore, some profiles showed a more significant reduction in salinity near the seafloor, which may indicate the seawater salinity effect of FSGD mixing with seawater in the seafloor interphase at a later stage, like that observed by Cardenas et al. (2010). ^{224}Ra and ^{228}Ra activities, the most commonly applied tracer of SGD[12], also suggest the existence of SGD at

the coastal areas of the study site (in the first 500 m from the coast). The results of Ra isotopes are comparable to the ones obtained by Diego-Feliu et al. (2022), who quantified the discharge of FSGD and identified that it is highly influenced by precipitation regimes (i.e. groundwater recharge). This is consistent with increased concentrations of Ra isotopes in seawater (i.e. increased SGD) following significant rainfall events resulting from elevated hydraulic pressure in the coastal aquifer, which mobilizes pre-existing groundwater towards offshore discharge zones. Although these measurements are not made directly in pore water, these results suggest that FSGD occurs in the areas identified by the MCRP. This assumption is consistent with data measured inland in which the alternation of highly transmissive layers with less permeable ones that act as a vertical barrier[33] favors the occurrence of FSGD hundreds of meters offshore. This assumption is also confirmed by Goyetche et al. 2023 from the interpretation of the tidal signal measured in the aquifer.

Seasonal resistivity changes associated with SGD and its importance

Through a comparative analysis of electrical resistivity models carried out during dry and wet campaigns, seasonal variations have been observed, with resistivity generally increasing during the rainy season as compared to the dry season. Data collected from piezometric levels have shown the influence of seasonal rainfall on aquifer recharge, leading to an increase in groundwater levels inland. The piezometer located at the mouth of the ephemeral Argentona stream, which is the closest point to where salinity profiles are conducted, shows a rise in aquifer level in response to rainfall events. This increase suggests that heightened hydraulic pressure mobilizes existing groundwater in the coastal aquifer towards the sea, resulting in amplified FSGD. To evidence this, model resistivity data over dry and wet seasons has been compared (Fig. 9). Looking at the distribution of resistivity values, a wider range of resistivity values is distinguished during the rainy season than the dry season, suggesting changes in the dynamics of groundwater flow during periods of higher precipitation and recharge. This is particularly evident in the sectors corresponding to transects V1, V2, V3, V5 and V7 (Figure SI2). However, this effect is less pronounced in transects V4 and V6, highlighting the importance of intrinsic geological and hydrogeological heterogeneity in the continuum of groundwater and ocean.

The Ra data establish a relationship between groundwater discharge and recharge rates, as observed by higher Ra concentrations during wet periods, consistent with the results of Diego-Feliu et al. (2022). This evidence aligns with findings from MCRP studies, which suggest an increase in discharge during the rainy season. MCRP data and Ra analysis corroborate the notion that groundwater discharge rates exhibit seasonal variability, with elevated discharge levels during periods of increased recharge verified by observation. This relationship between MCRP and Ra data underscores the importance of using complementary methodologies to comprehensively understand the dynamics of submarine groundwater discharge into coastal aquifers.

Implications for SGD studies

The application of MCRP techniques to SGD studies enhances our hydrogeological understanding and provides valuable insights across various scientific disciplines focused on the marine environment. MCRP seasonal surveys serve as an exploratory tool, effectively delineating areas with and without FSGD as well as temporal changes. Beyond hydrogeological research, in which preferential aquifer discharge areas are identified (i.e. higher groundwater resources), contributes fundamental scientific understanding to other disciplines, such as ecology, marine biology, and geochemistry; as well as providing a guide for resource allocation; focusing scientific inquiries; and fostering interdisciplinary collaboration. Additionally, seasonal MCRP studies complement quantification research, particularly when combined with other methods like radium (Ra) isotope studies and hydrogeological models. By capturing temporal dynamics, these studies contribute to a more robust understanding of FSGD, emphasizing the necessity for continuous research to comprehend temporal variations in coastal aquifers. This holistic approach aids in improving quantification studies, crucial for accurately assessing the impacts of FSGD.

Conclusions

In this work, we have assessed the use of marine continuous resistivity profiling (MCRP) as a method to identify areas of fresh submarine groundwater discharge (FSGD) and to evaluate their seasonal variations. The method has been tested in a detrital aquifer in the Maresme marine area, identifying seasonal differences in the electrical resistivity of the seabed up to 800 m offshore. The cited changes do not occur uniformly along transects or throughout the study area, evidencing the behavior of FSGD at the local and regional scales.

MCRP has been compared and validated with other independent methods, such as salinity profiles and the use of Ra isotopes, a widely applied method for quantifying SGD. The salinity profiles along transects V2, V6 and V7 show relatively lower values near the coast and salinity progressively increases offshore (38.0–38.6 PSU), corroborating the results of the electrical resistivity models. Similarly, isotopes ^{224}Ra and ^{228}Ra show a similar trend up to 500 m from the coastline. Finally, MCRP models are consistent with the results of different surveys carried out in order to characterize the aquifer on land.

Lastly, this study allows us to define the spatial distribution of FSGD changes that take place not only close to the coastline but hundreds of meters offshore, despite being in a detrital system. These spatial and seasonal variations must be considered when quantifying SGD volumes and their impact on the marine ecosystem.

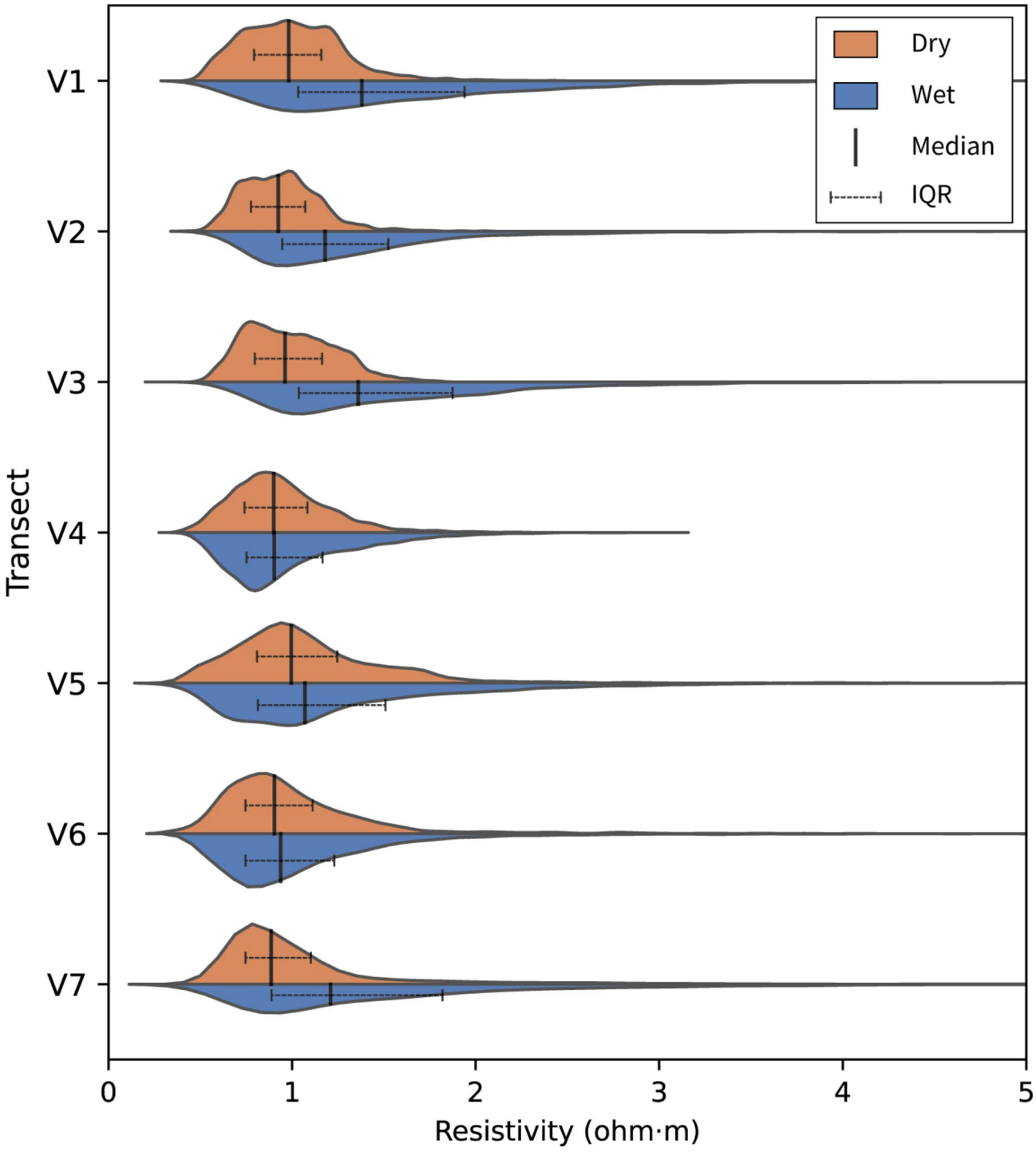

Fig. 9. Comparison of resistivity data (ohm·m) histograms obtained from the June 2020 (red) and October 2020 (blue) campaigns. The x-axis represents resistivity values (ohm·m), while the y-axis indicates the relative frequency of occurrence of those values in the electrical resistivity models.

Data availability

The findings of this study are supported by publicly available data accessible online at: https://doi.org/10.5281/zenodo.11389411.

Received: 29 May 2024; Accepted: 9 October 2024
Published online: 22 October 2024

References

1. Rodellas, V. et al. Submarine groundwater discharge as a major source of nutrients to the Mediterranean Sea. *Proc. Natl. Acad. Sci. U S A*. **112**, (2015).
2. Trezzi, G. et al. Submarine groundwater discharge: A significant source of dissolved trace metals to the North Western Mediterranean Sea. *Mar. Chem*. **186**, (2016).
3. Santos, I. R. et al. Submarine groundwater discharge impacts on coastal nutrient biogeochemistry. *Nat. Rev. EarthEnviron*. **2**. https://doi.org/10.1038/s43017-021-00152-0 (2021).
4. Alorda-Kleinglass, A. et al. The social implications of submarine groundwater discharge from an ecosystem services perspective: A systematic review. *Earth-Sci. Rev*. **221**. https://doi.org/10.1016/j.earscirev.2021.103742 (2021).
5. Lecher, A. L. & Mackey, K. R. M. Synthesizing the effects of submarine groundwater discharge on Marine Biota. *Hydrology*. **5**. https://doi.org/10.3390/hydrology5040060 (2018).
6. Moore, W. S. The effect of submarine groundwater discharge on the ocean. *Ann. Rev. Mar. Sci.* **2**, (2010).
7. Burnett, W. C., Bokuniewicz, H., Huettel, M., Moore, W. S. & Taniguchi, M. Groundwater and pore water inputs to the coastal zone. *Biogeochemistry*. **66**. https://doi.org/10.1023/B:BIOG.0000006066.21240.53 (2003).
8. Luijendijk, E., Gleeson, T. & Moosdorf, N. Fresh groundwater discharge insignificant for the world's oceans but important for coastal ecosystems. *Nat. Commun*. **11**, (2020).
9. Santos, I. R., Eyre, B. D. & Huettel, M. The driving forces of porewater and groundwater flow in permeable coastal sediments: A review. *Estuar. Coast. Shelf Sci*. **98**. https://doi.org/10.1016/j.ecss.2011.10.024 (2012).
10. Holliday, D., Stieglitz, T. C., Ridd, P. V. & Read, W. W. Geological controls and tidal forcing of submarine groundwater discharge from a confined aquifer in a coastal sand dune system. *J. Geophys. Res. Oceans* **112**, (2007).
11. Cantarero, D. L. M., Blanco, A., Cardenas, M. B., Nadaoka, K. & Siringan, F. P. Offshore submarine groundwater discharge at a coral reef front controlled by faults. *Geochem. Geophys. Geosyst.* **20**, (2019).
12. Garcia-Orellana, J. et al. Radium isotopes as submarine groundwater discharge (SGD) tracers: Review and recommendations. *Earth-Sci. Rev*. **220**. https://doi.org/10.1016/j.earscirev.2021.103681 (2021).
13. Taniguchi, M. et al. Submarine groundwater discharge: updates on its measurement techniques, geophysical drivers, magnitudes, and effects. *Front. Environ. Sci*. **7**. https://doi.org/10.3389/fenvs.2019.00141 (2019).
14. Jou-Claus, S., Folch, A. & Garcia-Orellana, J. Applicability of Landsat 8 thermal infrared sensor for identifying submarine groundwater discharge springs in the Mediterranean Sea basin. *Hydrol. Earth Syst. Sci.***25**, (2021).
15. Schubert, M. et al. Evidence for submarine groundwater discharge into the black sea-Investigation of two dissimilar geographical settings. *Water (Switzerland)* **9**, (2017).
16. Wilson, J. & Rocha, C. Regional scale assessment of submarine groundwater discharge in Ireland combining medium resolution satellite imagery and geochemical tracing techniques. *Remote Sens. Environ.* **119**, 21–34 (2012).
17. Stieglitz, T. C., Cook, P. G. & Burnett, W. C. Inferring coastal processes from regional-scale mapping of 222Radon and salinity: Examples from the Great Barrier Reef, Australia. *J. Environ. Radioact.* **101**, 544–552 (2010).
18. Rodellas, V. et al. Groundwater-driven nutrient inputs to coastal lagoons: The relevance of lagoon water recirculation as a conveyor of dissolved nutrients. *Sci. Total Environ.* **642**, 764–780 (2018).
19. Paepen, M., Hanssens, D., De Smedt, P., Walraevens, K. & Hermans, T. Combining resistivity and frequency domain electromagnetic methods to investigate submarine groundwater discharge in the littoral zone. *Hydrol. Earth Syst. Sci.* **24**, (2020).
20. Zarroca, M. et al. Delineating coastal groundwater discharge processes in a wetland area by means of electrical resistivity imaging, 224Ra and 222Rn. *Hydrol. Process* **28**, (2014).
21. Falgàs, E. et al. Integrating hydrogeological and geophysical methods for the characterization of a deltaic aquifer system. *Surv. Geophys.* **32**, (2011).
22. Palacios, A. et al. Time-lapse cross-hole electrical resistivity tomography (CHERT) for monitoring seawater intrusion dynamics in a Mediterranean aquifer. *Hydrol. Earth. Syst. Sci.* **24**, (2020).
23. Taniguchi, M., Ishitobi, T., Burnett, W. C. & Wattayakorn, G. Evaluating ground water-sea water interactions via resistivity and seepage meters. *Ground Water*. **45**, (2007).
24. Henderson, R. D. et al. Marine electrical resistivity imaging of submarine groundwater discharge: sensitivity analysis and application in Waquoit Bay, Massachusetts, USA. *Hydrogeol. J*. **18**, (2010).
25. Day-Lewis, F. D., White, E. A., Johnson, C. D., Lane, J. W. & Belaval, M. Continuous resistivity profiling to delineate submarine groundwater discharge - Examples and limitations. *Leading Edge (Tulsa, OK)* **25**, (2006).
26. Cardenas, M. B. et al. Linking regional sources and pathways for submarine groundwater discharge at a reef by electrical resistivity tomography, 222Rn, and salinity measurements. *Geophys. Res. Lett.* **37**, (2010).
27. Befus, K. M., Cardenas, M. B., Tait, D. R. & Erler, D. V. Geoelectrical signals of geologic and hydrologic processes in a fringing reef lagoon setting. *J. Hydrol. (Amst)* **517**, (2014).
28. Swarzenski, P. W. & Izbicki, J. A. Coastal groundwater dynamics off Santa Barbara, California: Combining geochemical tracers, electromagnetic seepmeters, and electrical resistivity. *Estuar. Coast. Shelf Sci.* **83**, (2009).
29. Breier, J. A., Breier, C. F. & Edmonds, H. N. Detecting submarine groundwater discharge with synoptic surveys of sediment resistivity, radium, and salinity. *Geophys. Res. Lett.* **32**, (2005).
30. Colombo, F. & Rivero, L. Quaternary over-elevated torrential channels. Characteristics and depositional significance: the Maresme model (Catalonia, NE Spain). *Int. J. Earth Sci.* **106**, (2017).
31. Cisteró, X. F. & Camarós, J. G. Les rierades al Maresme. *L'Atzavara* **23**, 61–79 (2014).
32. Reventós, J. S. Els condicionants geomorfològics de les praderies de posidònia del Maresme. *L'Atzavara* **10**, 7–10 (2002).
33. Google LLC. (2024). Google Earth Pro (version 7.3.6.9796). Available at https://www.google.com/earth/versions/. Accessed 8 March 2024.
34. Martínez-Pérez, L. et al. A multidisciplinary approach to characterizing coastal alluvial aquifers to improve understanding of seawater intrusion and submarine groundwater discharge. *J. Hydrol. (Amst)* **607**, (2022).
35. Goyetche, T. et al. Using the tidal method to develop a conceptual model and for hydraulic characterization at the Argentona research site, NE Spain. *Hydrogeol. J.* **31**, (2023).
36. Folch, A. et al. Combining fiber optic DTS, cross-hole ERT and time-lapse induction logging to characterize and monitor a coastal aquifer. *J. Hydrol. (Amst)* **588**, (2020).
37. Diego-Feliu, M. et al. Extreme precipitation events induce high fluxes of groundwater and associated nutrients to coastal ocean. *Hydrol. Earth Syst. Sci.* **26**, (2022).
38. Servei Meteorològic de Catalunya: Catàleg de dades, https://www.meteo.cat/wpweb/serveis/cataleg-de-serveis/dades-meteorologiques/. Accessed 24 Oct 2022.
39. Moore, W. S. & Reid, D. F. Extraction of radium from natural waters using manganese-impregnated acrylic fibers. *J. Geophys. Res.* **78**, (1973).
40. Sun, Y. & Torgersen, T. The effects of water content and Mn-fiber surface conditions on 224Ra measurement by 220Rn emanation. *Mar. Chem.* **62**, (1998).
41. Moore, W. S. & Arnold, R. Measurement of223Ra and224Ra in coastal waters using a delayed coincidence counter. *J. Geophys. Res. Oceans* **101**, (1996).
42. Diego-Feliu, M. et al. Guidelines and limits for the quantification of Ra isotopes and related radionuclides with the radium delayed coincidence counter (RaDeCC). *J. Geophys. Res. Oceans* **125**, (2020).

43. Garcia-Solsona, E., Garcia-Orellana, J., Masqué, P. & Dulaiova, H. Uncertainties associated with 223Ra and 224Ra measurements in water via a delayed coincidence counter (RaDeCC). *Mar. Chem.* **109**, (2008).
44. Dimova, N. T., Swarzenski, P. W., Dulaiova, H. & Glenn, C. R. Utilizing multichannel electrical resistivity methods to examine the dynamics of the fresh water-seawater interface in two Hawaiian groundwater systems. *J. Geophys. Res. Oceans.* **117**, (2012).
45. Archie, G. E. The electrical resistivity log as an aid in determining some reservoir characteristics. *Trans. AIME.* **146**, (1942).
46. Belaval, M., Lane, J. W., Lesmes, D. P. & Kineke, G. C. Continuous-resistivity profiling for coastal ground-water investigations: Three case studies. in (2003). https://doi.org/10.4133/1.2923186.
47. Manzanera, M. & Cardell, M. J. Cartografia de Posidònia oceànica davant les costes de Mataró. *L'Atzavara* **10**, 11–22 (2002).
48. Psomiadis, D., Tsourlos, P. & Albanakis, K. Electrical resistivity tomography mapping of beachrocks: Application to the island of Thassos (N. Greece). *Environ. Earth Sci.* **59**, (2009).
49. Tovar-Sánchez, A. et al. Contribution of groundwater discharge to the coastal dissolved nutrients and trace metal concentrations in Majorca Island: Karstic vs detrital systems. *Environ. Sci. Technol.* **48**, (2014).

Acknowledgements

The authors would like to thank all colleagues from the Grup d'Hidrologia Subterrània - GHS (Universitat Politècnica de Catalunya) funded with the grant Agaur-SGR-609 and from the Grup de Recerca en Radioactivitat Ambiental de Barcelona – GRAB (Universitat Autònoma de Barcelona), for participating in the sampling campaigns. This research has been supported by the Catalan Water Agency (grant no. ACA210/18/00007) and the project PID2022-140862OB-C21 funded by MCIN/AEI/10.13039/501100011033/ and "FEDER Una manera de hacer Europa". J. Tur-Piedra acknowledges the economic support from the FI-2022 fellowships of the Generalitat de Catalunya autonomous government (2022FI_B_00601). M. Diego-Feliu acknowledges financial support from grant JDC2022-050316-I funded by MCIN/AEI/10.13039/501100011033 and by the European Union - NextGenerationEU/PRTR.

Author contributions

J.T.-P. oversaw the conceptualization of the study, developed the methodological approaches including sampling campaigns and the investigation of previous works and literature, and prepared the manuscript. J.L. contributed to the study's conceptualization, sampling, and development of the geophysical technique. M.D.-F. was involved in the study conceptualization, sampling, laboratory work, and the revision and editing of the manuscript. P.Q. assisted with the development of the geophysical technique, conducted the statistical data analysis, and reviewed the manuscript. A.M. also supported the development of the geophysical technique, carried out the statistical data treatment, and reviewed the manuscript. V.R. contributed to the study conceptualization and the revision and editing of the manuscript. A.F. oversaw the study conceptualization, developed the methodological approaches, revised and edited various drafts, supervised and administered the research project, and secured funding.

Declarations

Competing interests

The authors declare no competing interests.

Additional information

Supplementary Information The online version contains supplementary material available at https://doi.org/10.1038/s41598-024-75984-z.

Correspondence and requests for materials should be addressed to J.T.-P.